^{57}Fe Mössbauer and x-ray magnetic circular dichroism study of magnetic compensation of the rare-earth sublattice in $Nd_{2-x}Ho_xFe_{14}B$ compounds

J. Chaboy,[1] C. Piquer,[1] N. Plugaru,[1,*] F. Bartolomé,[1] M. A. Laguna-Marco,[2] and F. Plazaola[3]
[1]*Instituto de Ciencia de Materiales de Aragón, CSIC-Universidad de Zaragoza, 50009 Zaragoza, Spain*
[2]*CITIMAC, Universidad de Cantabria, Avenida de los Castros s/n, 39005 Santander, Spain*
[3]*Departamento de Electricidad y Electrónica, Universidad del País Vasco (UPV/EHU), Apartado 644, 48080 Bilbao, Spain*
(Received 30 April 2007; revised manuscript received 27 August 2007; published 10 October 2007)

We present here a study of the magnetic properties of the $Nd_{2-x}Ho_xFe_{14}B$ series. The macroscopic properties of these compounds evolve continuously from those of $Nd_2Fe_{14}B$ to those of $Ho_2Fe_{14}B$ as Ho gradually replaces Nd. The system shows a compensation of the rare-earth sublattice magnetization for a critical concentration, $x_c=0.55$, that is reflected into the anomalous behavior of both macroscopic and microscopic magnetic probes. The combined analysis of magnetization, ^{57}Fe Mössbauer spectroscopy and Fe *K*-edge x-ray magnetic circular dichroism (XMCD) measurements suggests that the origin of the anomalous magnetic behavior found at $x_c=0.55$ is mainly due to the Ho sublattice. Moreover, the analysis of the Fe *K*-edge XMCD signals reveal the presence of a rare-earth contribution, reflecting the coupling of the rare-earth and Fe magnetic moments, which can lead to the possibility of disentangling the magnetic behavior of both Fe and R atoms using a single absorption edge.

DOI: 10.1103/PhysRevB.76.134408 PACS number(s): 61.10.Ht, 76.80.+y, 71.20.Lp, 75.50.Bb

I. INTRODUCTION

In the past years we have witnessed the development and consolidation of the x-ray magnetic circular dichroism (XMCD)[1] as a powerful tool for microscopic magnetic characterization. XMCD incorporates the inherent advantage of x-ray absorption spectroscopy, that of being element and shell specific, to study magnetic effects. The derivation of the so-called sum rules,[2,3] showing the relationship of the XMCD to the local spin and orbital magnetic moments, triggered an enormous interest into applying XMCD to basic and applied research on magnetism. XMCD can be particularly suitable to study those phenomena hidden to macroscopic techniques.

This is the case of rare-earth-iron (*R*-Fe) intermetallic compounds in which the detailed knowledge of the mechanism coupling the magnetic properties of both *R* and Fe sublattice needs the magnetic characterization of the *R*-5*d* states. However, the experiments performed at the rare-earth $L_{2,3}$ edges show that the interpretation of XMCD at the $L_{2,3}$ edges of the lanthanides is not so straightforward as for the 3*d* transition metals.[4–7] On the other hand, different experimental XMCD works performed at the Fe *K* edge in *R*-Fe intermetallic compounds have shown the influence of the rare-earth magnetism into the dichroic spectra.[8–11] The rare-earth contribution to the Fe *K*-edge XMCD not only reflects the magnetic state of the *R* atoms but also bears information on the coupling of the rare-earth magnetic moment to that of Fe. As a consequence, the correct identification of this rare-earth contribution would allow us to disentangle, using a single absorption edge, the magnetic behavior of both Fe and *R* atoms.

Aimed to verify this proposition we have tailored a systematic study of the $Nd_{2-x}Ho_xFe_{14}B$ series, in which Ho gradually replaces Nd, by means of magnetization, ^{57}Fe Mössbauer spectroscopy and Fe *K*-edge XMCD measurements. The $R_2Fe_{14}B$ intermetallic compounds have been the subject of a great activity due their permanent-magnet properties.[12–15] The complicated interplay of exchange and crystal field interactions in these systems aimed numerous studies from a macroscopic point of view. However, the behavior of the magnetic moments at the microscopic scale is less understood, specially concerning the magnetic arrangement of the rare-earth and Fe moments in the low-temperature phase. The collinearity between the magnetic moments in $Nd_2Fe_{14}B$ in the low-temperature phase has been a subject of study and controversy for a long time,[12,16,17] and only the use of microscopic techniques as XMCD and x-ray resonant magnetic scattering has provided a definitive answer.[18–20]

In the $Nd_{2-x}Ho_xFe_{14}B$ compounds the Fe magnetic moments are ferromagnetically coupled to those of Nd, while the coupling is ferrimagnetic with respect to the Ho moments. Therefore, the rare-earth contribution to the Fe *K*-edge XMCD would vary in both sign and amplitude as a function of the Ho concentration, making possible the disentangling of the Nd and Ho contribution to the XMCD spectra. The detailed study of the XMCD signals shows that the rare-earth contribution is not equivalent to that of an effective rare-earth magnetization but it preserves the atomic nature and the characteristic magnetic coupling of each rare-earth species.

II. EXPERIMENT

$Y_2Fe_{14}B$ and the $Nd_{2-x}Ho_xFe_{14}B$ alloys ($x=0$, 0.2, 0.4, 0.5, 0.55, 0.6, 0.8, 1.2, 1.6, and 2) were prepared by melting the pure elements in a high-frequency induction furnace, under Ar protective atmosphere. The as-cast alloys were wrapped in Ta foil and enclosed in silica tubes, under Ar gas. All the samples were annealed at 950 °C for two weeks and then quenched to room temperature. Structural characterization was performed at room temperature (RT) by means of

powder x-ray diffraction, using a rotating-anode Rigaku diffractometer in the Bragg-Brentano geometry, with Cu $K\alpha$ radiation. The diffraction patterns were Rietveld refined using the FULLPROF code.[21] All the studied compounds exhibit the $Nd_2Fe_{14}B$-type structure ($P4_2/mnm$ space group). In all the cases the presence of secondary phases (α-Fe) is less than 3% overall.

The macroscopic magnetic measurements were performed by using a commercial superconducting quantum interference device magnetometer (Quantum Design MPMS-S5). Magnetization isotherms were measured on loose powders in applied magnetic fields $H \leqslant 50$ kOe. The Curie temperature, T_C, was determined from thermomagnetic curves measured with a Faraday-type balance between RT and 1073 K, using Ni standard as reference. T_C was determined at the inflection point of the $M(T)$ drop at high temperature. The Mössbauer spectra were measured at RT by using a constant-acceleration spectrometer which uses a rhodium matrix ^{57}Co source and was calibrated with an α-Fe foil. The thickness of the Mössbauer absorber was optimized, ~ 30 mg/cm^2, in order to improve the absorption line resolution.

X-ray magnetic circular dichroism measurements were performed at the beamline BL39XU of the SPring8 Facility.[22] Undulator radiation, linearly polarized in the orbit plane, was monochromatized by a Si(111) fixed-exit double-crystal monochromator and higher harmonics rejected by a Pt coated mirror. Circularly polarized x rays were generated using a 0.73 mm thick diamond x-ray phase plate.[23] The degree of circular polarization is >90% in the energy range of our interest. Fe K-edge XMCD measurements of the $Nd_{2-x}Ho_xFe_{14}B$ and $Y_2Fe_{14}B$ compounds were carried out at room temperature and under the action of an applied magnetic field of 50 kOe. XMCD spectra were recorded in the transmission mode using the helicity-modulation technique.[24] Therefore, the sample is magnetized by an external magnetic field, applied in the direction of the incident beam, and the helicity is changed from positive to negative at each energy point. Consequently, XMCD spectra are obtained without reversing the applied magnetic field. The XMCD spectrum corresponds to the spin-dependent absorption coefficient obtained as the difference of the absorption coefficient $\mu_c=(\mu^- - \mu^+)$ for antiparallel, μ^-, and parallel, μ^+, orientations of the photon helicity and the magnetic field applied to the sample. For the sake of accuracy the direction of the applied magnetic field is reversed and XMCD, now $\mu_c=(\mu^+ - \mu^-)$, is recorded again by switching the helicity. The substraction of the XMCD spectra recorded for both field orientations cancels, if present, any spurious signal.

We have adopted the same convention for the sign of the circular dichroism as in Ref. 2, i.e., with the quantization axis determined by the direction of the Fe majority spin. It should be noted that the magnetization of the Fe sublattice is always dominant for both $Y_2Fe_{14}B$ and $Nd_{2-x}Ho_xFe_{14}B$ systems. For the XMCD measurements, homogeneous layers of the samples were made by spreading of fine powders of the material on an adhesive tape. Thickness and homogeneity of the samples were optimized to obtain the best signal-to-noise ratio. The absorption spectra were analyzed according to standard procedures.[25] The origin of the energy scale, E_0, was defined as the inflection point of the absorption edge. The spectra were normalized to the averaged absorption coefficient at high energy, μ_0, in order to eliminate the dependence of the absorption on the sample thickness.

TABLE I. Structural parameters of the $Nd_{2-x}Ho_xFe_{14}B$ compounds: lattice constants a and c, a/c ratio, and unit-cell volume (V).

x	a (Å)	c (Å)	a/c	V (Å^3)
0	8.7972(3)	12.1901(7)	0.7217	943.4(1)
0.2	8.7919(4)	12.1687(10)	0.7225	940.6(1)
0.4	8.7928(3)	12.1587(7)	0.7232	940.0(1)
0.5	8.7956(2)	12.1518(7)	0.7238	940.1(1)
0.55	8.7798(4)	12.1182(9)	0.7245	934.1(1)
0.55[S2]	8.7751(4)	12.1198(9)	0.7240	933.3(1)
0.6	8.7944(3)	12.1426(7)	0.7243	939.1(1)
0.8	8.7735(5)	12.0998(13)	0.7251	931.4(1)
1.2	8.7645(4)	12.0626(10)	0.7266	926.6(1)
1.6	8.7478(5)	12.0034(14)	0.7288	918.5(1)
2	8.7368(3)	11.9701(8)	0.7299	913.7(1)

III. RESULTS AND DISCUSSION

A. Macroscopic structural and magnetic characterization

The $Nd_{2-x}Ho_xFe_{14}B$ compounds show a tetragonal unit cell with six different crystallographic positions for Fe ($16k_1$, $16k_2$, $8j_1$, $8j_2$, $4e$, and $4c$), two for Nd ions ($4f$ and $4g$), and one for B ($4g$).[12] The lattice constants, a/c ratio, and unit-cell volume are summarized in Table I. The cell parameters decrease as the Ho content increases through the $Nd_{2-x}Ho_xFe_{14}B$ series (see Fig. 1). The contraction of the crystal cell as the Ho content, x, increases from 0 to 2 is anisotropic: 0.8% and 1.9% along the a and c axes, respectively. Surprisingly, both a and c lattice parameters show a marked reduction for $x=0.55$, which is also reflected into the cell volume dependence. A second sample (S2) with $x=0.55$ concentration was prepared in order to confirm this result. As shown in Fig. 1, the refined values of the lattice constants are reproducible for the $Nd_{1.45}Ho_{0.55}Fe_{14}B$ samples of different batches.

The temperature dependence of the magnetization through the $Nd_{2-x}Ho_xFe_{14}B$ series is shown in Fig. 2. Both $Nd_2Fe_{14}B$ and $Ho_2Fe_{14}B$ display uniaxial magnetic anisotropy at RT with the easy direction of magnetization (EMD) lying along the tetragonal c axis. Below RT these compounds exhibit spin-reorientation transitions (SRTs) at which the magnetization cants away from the c-axis direction with an angle that increases with decreasing temperature.[16,17] These transitions are characterized by an abrupt change in the magnetization vs temperature curve, $M(T)$, at the onset of the SRT.[26,27]

As shown in Fig. 2, the substituted $Nd_{2-x}Ho_xFe_{14}B$ compounds exhibit similar $M(T)$ behavior as that of $Nd_2Fe_{14}B$ and $Ho_2Fe_{14}B$. Noticeably, the jump of the magnetization at T_{SRT} is less marked for the $x=0.5$ and 0.6 compounds. This result seems to be related with the dependence of T_{SRT} on the Ho concentration. The temperature of the onset of the SRT

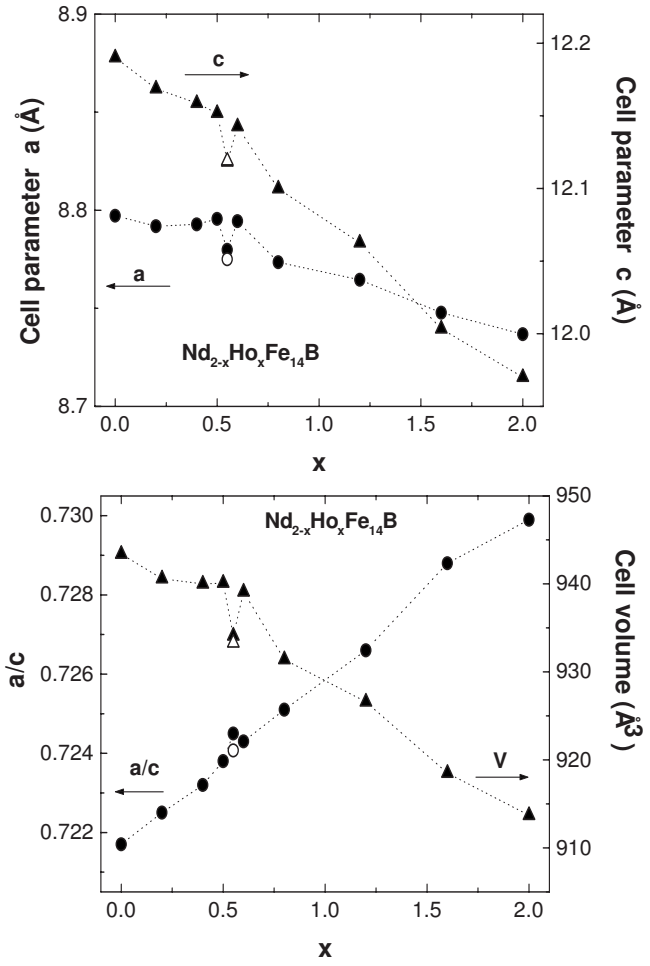

FIG. 1. Top panel: composition dependence of the lattice constants a (●) and c (▲) through the $Nd_{2-x}Ho_xFe_{14}B$ series. Bottom panel: the same comparison is shown for the a/c ratio (●) and the cell volume (▲). The open symbols correspond to the S2 ($x=0.55$) sample (see text for details).

transition, T_{SRT}, has been determined as the inflection point of the $M(T)$ curves measured in the presence of an applied field of 1 kOe (see Table II). As shown in Fig. 2, T_{SRT} decreases as the Ho content increases. However, this decrease is not linear but showing a different trend for compounds with $x \leqslant 0.45$ and $x \geqslant 0.50$. Moreover, the T_{SRT} of the $x=0.55$ compound follows the same dependence as the low Ho content samples.

These results are tentatively addressed to the different substitution of Nd by Ho at the $4f$ and $4g$ sites. In the case of $Nd_2Fe_{14}B$ the $4g$ site prefers the [001] direction at ambient temperature and dictates the macroscopic easy-axis direction. On the contrary, the $4f$ site reduces the intrinsic stability by favoring alignment along [110]-type directions.[20] As a consequence, the competition between the rare-earth magnetic anisotropy at both $4f$ and $4g$ sites controls the SRT transition. On the basis of the R-atom size and lattice site volume[12,13] one may assume that Ho preferentially substitutes Nd at the $4f$ sites. For $x<0.5$ all the $4g$ sites are occupied by Nd ions and there are more Nd atoms than Ho ones at the $4f$ sites. For $0.5 \leqslant x \leqslant 1$ the Nd vs Ho occupancy of the $4f$ sites is reversed and Ho should dominate the contribution of the $4f$ sites to the magnetic anisotropy. However, it should be noted that the R-Fe exchange is larger for the light R than for the heavy R.[12] Consequently, the peculiar behavior of $M(T)$ for $x=0.5$ and $x=0.6$ may be addressed to the competition between the Nd and Ho ions into determining the magnetic anisotropy of the $4f$ sites. Within this frame, the fact that the T_{SRT} of the $x=0.55$ compound follows the same dependence as the low Ho content samples should indicate an unexpected smaller contribution of Ho to this competition.

Further confirmation of the different R-Fe exchange for Nd and Ho ions can be obtained from the analysis of the Curie temperatures. According to previous findings in the $R_2Fe_{14}B$ series, T_C exhibits a smooth ($\sim G^{1/2}$) dependence with the de Gennes factor (G) that is different for light R and heavy R. This behavior has been interpreted in terms of the larger R-Fe exchange for the light R than for the heavy rare earths since the exchange interactions between $4f$ and $5d$ electrons are larger for light-R elements due to a smaller difference between the spatial extent of $4f$ and $5d$ shells.[12,13] The variation of T_C on the Ho concentration through the $Nd_{2-x}Ho_xFe_{14}B$ series reported in Fig. 2 shows that T_C decreases as the Ho content increases. However, a different T_C vs x dependence is found for compounds in which $x \leqslant 1.2$ and those with $x \geqslant 1.6$, i.e., for the Nd-rich and Ho-rich compounds. According to the preferential substitution scheme discussed above, this change of behavior takes place at $x \sim 1.5$, i.e., when Ho ions occupy all the $4f$ sites and, in addition, there are more Ho atoms than Nd ones at the $4g$ sites. In other words, the change of the T_C dependence takes place when Ho dominates the anisotropy of both $4f$ and $4g$ sites within the $Nd_{2-x}Ho_xFe_{14}B$ series.

The concentration dependence of the cell parameters (Table I), $M(T)$ (Fig. 2), and T_{SRT} (Table II) through the $Nd_{2-x}Ho_xFe_{14}B$ series indicates the peculiarity of the region close to $x=0.55$. The singular behavior of the $Nd_{1.45}Ho_{0.55}Fe_{14}B$ compound within the whole series is also reflected in the composition dependence of the magnetization as a function of magnetic applied field, $M(H)$. As shown in Fig. 3, the maximum of magnetization is found for the $Nd_2Fe_{14}B$ compound and the magnetization decreases as the Ho content increases so as to reach its minimum value for $Ho_2Fe_{14}B$. This behavior can be accounted in terms of the different magnetic coupling of both Nd and Ho magnetic moments with that of Fe. At room temperature, the magnetic moments of both Fe and Nd atoms are ferromagnetically coupled in $Nd_2Fe_{14}B$. By contrast, the coupling between μ_{Ho} and μ_{Fe} is ferrimagnetic in the case of $Ho_2Fe_{14}B$. Within a two-sublattice framework the magnetization of the $Nd_{2-x}Ho_xFe_{14}B$ compounds can be expressed as[28] $\vec{M}_{tot}=\vec{M}_{Fe}+\vec{M}_R$, being $\vec{M}_{Fe}=14\vec{\mu}_{Fe}$ and $\vec{M}_R=(2-x)\vec{\mu}_{Nd}+x\vec{\mu}_{Ho}$. Due to this coupling scheme μ_{Nd} and μ_{Ho} are ferrimagnetically coupled through the $Nd_{2-x}Ho_xFe_{14}B$ series and, consequently, the magnetization decreases as the Ho content increases. Beyond this general trend, the dependence with the Ho concentration of the magnetization measured in an applied magnetic field $\mu_0 H=5$ T, $M_{tot}(5\text{ T})$,[29] shows an unusual behavior (see Table II). As shown in Fig. 3, $M_{tot}(5\text{ T})$ decreases in a linear way as increasing x through the $Nd_{2-x}Ho_xFe_{14}B$ series, with the exception of the $x=0.55$

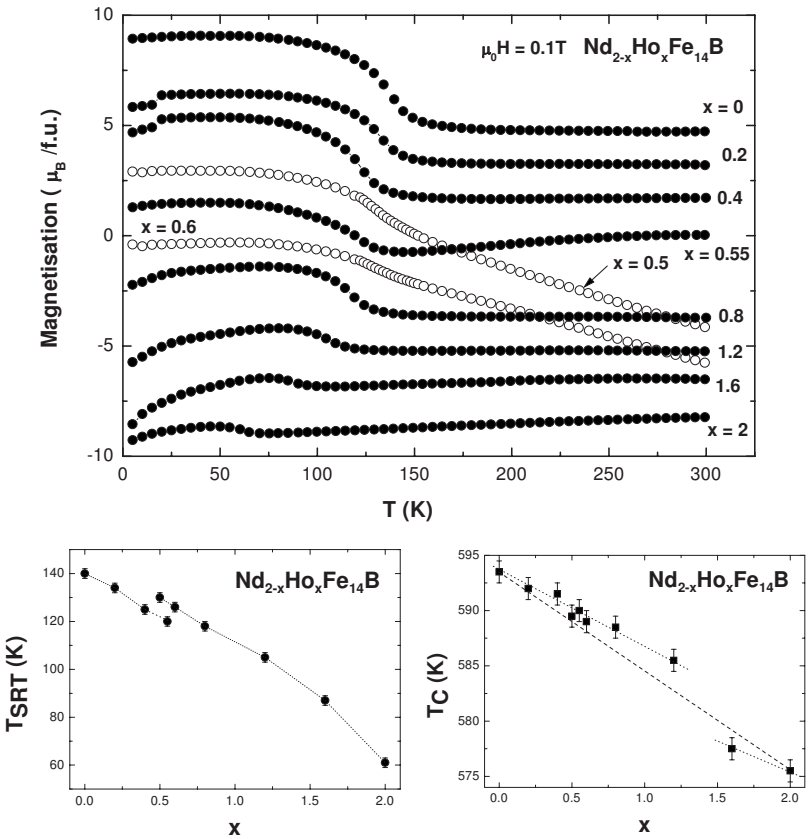

FIG. 2. Top panel: temperature dependence of the magnetization of the $Nd_{2-x}Ho_xFe_{14}B$ series measured under an applied magnetic field $H=1$ kOe. The scale is referred to the $x=0$ compounds and for the sake of clarity the curves have been vertically shifted. Bottom panels: concentration dependence of the spin reorientation (left) and Curie temperatures (right). In the right panel the dashed line is a guide to the eye showing the linear dependence.

compound for which $M_{tot}(5\ \mathrm{T})$ shows a sudden increase. This behavior is similar for the $M(H)$ curves recorded at both $T=4.2$ K and at RT.

We have applied a two-sub-lattice model in order to extract the magnetization of the rare-earth sublattice, M_R. It has been assumed that the magnetization of the Fe sublattice in the $Nd_{2-x}Ho_xFe_{14}B$ compounds corresponds to that of $Y_2Fe_{14}B$ recorded at the same conditions (temperature and applied magnetic field). In this way, M_R is obtained from the direct subtraction of the $Y_2Fe_{14}B$ magnetization to that of the $Nd_{2-x}Ho_xFe_{14}B$ compounds. It should be noted that at room temperature the reduced temperature, T/T_C, ranges from 0.51 for $Nd_2Fe_{14}B$ to 0.52 for $Ho_2Fe_{14}B$, being 0.52 that of $Y_2Fe_{14}B$. The obtained values of M_R have been compared with the rare-earth sublattice magnetization calculated as $M_{cal}=(2-x)\vec{\mu}_{\mathrm{Nd}}+x\vec{\mu}_{\mathrm{Ho}}$, where μ_{Nd} and μ_{Ho} have been determined by subtracting the $Y_2Fe_{14}B$ magnetization to that of the $Nd_2Fe_{14}B$ and $Ho_2Fe_{14}B$ compounds, respectively. The comparison between the rare-earth sublattice magnetization experimentally determined, M_R, and the calculated one, M_{cal},

TABLE II. Curie temperature (T_C), spin-reorientation temperature (T_{SRT}), and magnetic parameters of the $Nd_{2-x}Ho_xFe_{14}B$ compounds. $M_{tot}(5\ \mathrm{T})$ is the total magnetization at 5 T; M_R is the magnetization of the rare-earth sublattice and M_{cal} its calculated value (see text for details).

x	$M_{tot}(5\ \mathrm{T})$ 4.2 K	$M_{tot}(5\ \mathrm{T})$ 300 K	T_C	T_{SRT}	$M_R(5\ \mathrm{T})$ 4.2 K	$M_R(5\ \mathrm{T})$ 300 K	$M_{cal}(5\ \mathrm{T})$ 4.2 K	$M_{cal}(5\ \mathrm{T})$ 300 K
0	37.81	33.17	593.5	140	4.90	3.89	4.90	3.89
0.2	35.32	31.53	592	134	2.41	2.25	2.39	2.22
0.4	32.81	30.23	591.5	125	−0.10	0.95	−0.13	0.56
0.5	32.18	29.55	589.5	130	−0.73	0.27	−1.38	−0.27
0.55	32.60	30.20	590	120	−0.31	0.92	−2.01	−0.69
0.6	29.96	28.83	589	126	−2.95	−0.45	−2.64	−1.11
0.8	26.99	25.83	588.5	118	−5.92	−3.45	−5.15	−2.77
1.2	23.67	23.78	585.5	105	−9.24	−5.50	−10.18	−6.10
1.6	17.70	20.22	577.5	87	−15.21	−9.06	−15.21	−9.42
2	12.67	16.53	575.5	61	−20.24	−12.75	−20.24	−12.75
$Y_2Fe_{14}B$	32.91	29.28	574					

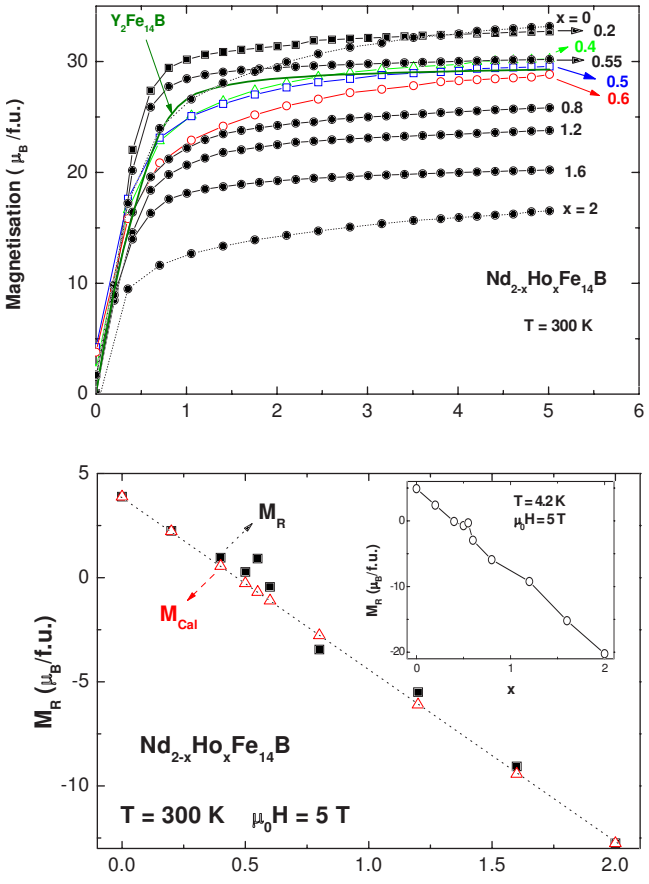

FIG. 3. (Color online) Top panel: magnetization vs applied magnetic field curves of the $Nd_{2-x}Ho_xFe_{14}B$ series recorded at room temperature. The $M(H)$ curve of $Y_2Fe_{14}B$ is also shown (solid line). Bottom panel: comparison of the concentration dependence of the rare-earth sublattice magnetization (M_R) obtained from the experimental $M(H)$ data at $\mu_0 H=5$ T (■), and that computed, M_{cal} (△), as the weighted sum of the rare-earth magnetization derived for $Nd_2Fe_{14}B$ and $Ho_2Fe_{14}B$ (see text for details). In the inset, the concentration dependence of M_R at $T=4.2$ K and $\mu_0 H=5$ T is shown.

shows a good agreement in the whole composition range except for the compound with $x=0.55$. In this case the calculated value is $M_{cal}=-0.69\ \mu_B$ while the experimental one is $M_R=0.92\ \mu_B$.

The peculiarity of the $x=0.55$ concentration within the $Nd_{2-x}Ho_xFe_{14}B$ series lies close to the expected value for the occurrence of the compensation of the rare-earth sublattice magnetization. As discussed above, the relative orientation of the M_{Fe} and M_R sublattice magnetizations depends through this series on the particular Ho concentration: it is parallel in the case of Nd-rich compounds $[(2-x)|\mu_{Nd}|>x|\mu_{Ho}|]$ and antiparallel in the Ho-rich side $[(2-x)|\mu_{Nd}|<x|\mu_{Ho}|]$ of the series. As a consequence, the orientation of $\vec{M}_R$ with respect to $\vec{M}_{Fe}$ is reversed for a critical concentration at which $(2-x)|\mu_{Nd}|=x|\mu_{Ho}|$ and $\vec{M}_R$ cancels. This behavior is equivalent to a magnetic-compensation phenomenon but referred to the rare-earth sublattice only. An estimate of the critical concentration, x_c, at which the compensation occurs can be obtained by assuming the free ion value for both μ_{Nd} ($3.27\ \mu_B$) and μ_{Ho} ($10\ \mu_B$). Under this approximation, $\vec{M}_R$ should be zero for $x=0.49$. This value cannot be directly compared to the room temperature data as the free ion approach is not longer valid and, in addition, the thermal dependence of the Nd and Ho magnetic moments may be different. Therefore, we have determined the critical concentration as $x_c=0.47$ by using the μ_{Nd} and μ_{Ho} values derived from the $M(H)$ data at room temperature. These values are close to that of $Nd_{1.45}Ho_{0.55}Fe_{14}B$, i.e., the compound showing a peculiar behavior within the series.

Trying to discern if the origin of such behavior is connected to the occurrence of a magnetic compensation within the rare-earth sublattice, we have applied two different microscopic techniques as ^{57}Fe Mössbauer spectroscopy and Fe K-edge XMCD. By using these atomic-selective techniques it would be possible to disentangle the dependence of the magnetic properties of the Fe sublattice on the Ho concentration. Moreover, they allow us to verify if the magnetization of the Fe sublattice remains unaltered through the whole $Nd_{2-x}Ho_xFe_{14}B$ series, as assumed in the two-sublattice analysis of the magnetization data. We have performed the study of both ^{57}Fe Mössbauer and Fe K-edge XMCD at room temperature. Working well above the temperature region in which the spin reorientation takes place guarantees that possible effects associated with the modification of the magnetic moments arrangement, due to the variation of the EMD, are minimized.

B. Analysis of the ^{57}Fe Mössbauer spectra

The Mössbauer spectra of the $Nd_{2-x}Ho_xFe_{14}B$ compounds, see Fig. 4, have been fitted with six sextets corresponding to the six crystallographic nonequivalent Fe sites of the $R_2Fe_{14}B$ structure.[30–33] In all cases a small amount of magnetic α-Fe has been included in the fit. Because its amount ($<3\%$) is known from the previous x-ray diffraction (XRD) analysis and the hyperfine parameters are known from the literature,[34] they have been included in the fit with no modification of the number of adjustable parameters.

The assignment of the six spectral components to the different crystallographic iron sites $16k_1$ (10, 1, 11.75), $16k_2$ (10, 0, 11.55), $8j_1$ (9, 0, 12.11), $8j_2$ (12, 0, 12.70), $4e$ (9, 2, 11.83), and $4c$ (8, 0, 12.30), is based upon their relative areas and near neighbor environment. The numbers in the parentheses are, respectively, the number of Fe (Z_{Fe}) and B (Z_B) near neighbors and the Wigner-Seitz volume [V_{WS}(Å^3)].[30] In general, the largest Z_{Fe} and V_{WS}, the largest the hyperfine field B_{hf} is. Moreover, in the case of the $R_2Fe_{14}B$ compounds it is considered that the B atoms behave as electron donors to the Fe atom, thus reducing the hyperfine field of the adjacent Fe atoms.[30,31] The largest value of B_{hf} is expected for the $8j_2$ site because it has $Z_B=0$ and the largest value of both the number of Fe near neighbors ($Z_{Fe}=12$) and Wigner-Seitz volume. For both $16k_1$ and $16k_2$ sites $Z_{Fe}=10$ and $V_{WS}(16k_1)>V_{WS}(16k_2)$. However, because $Z_B=1$ for the $16k_1$ site while it is zero for the $16k_2$ one, the second largest hyperfine field is expected for the $16k_2$ site. The smallest hyperfine field corresponds to one of the two weakest components, the $4c$ site with only eight Fe atoms near neighbors. The assignment of the remaining $16k_1$, $8j_1$, and $4e$ sites is

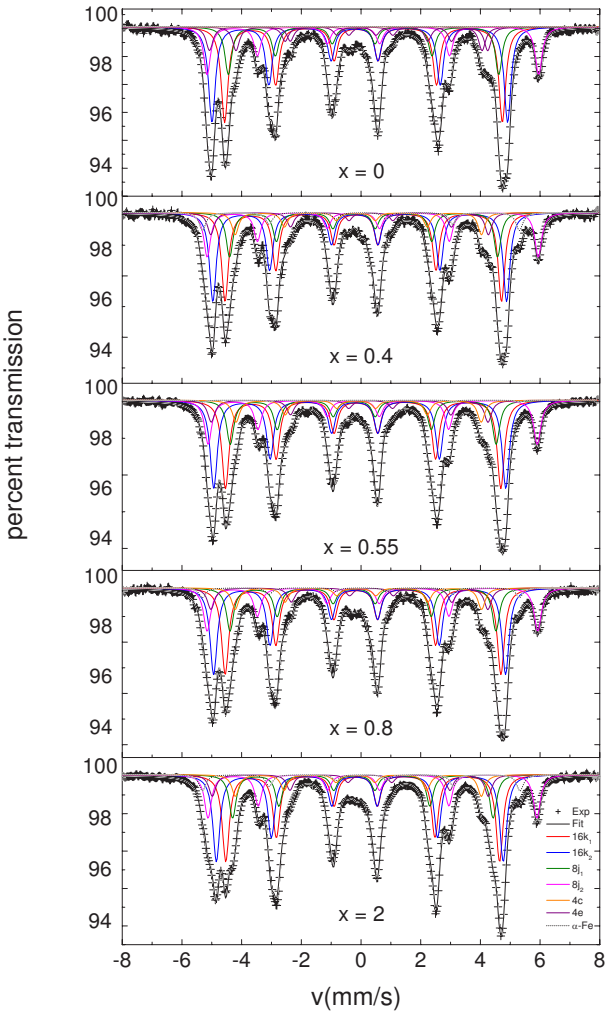

FIG. 4. (Color online) ^{57}Fe Mössbauer of $Nd_{2-x}Ho_xFe_{14}B$ compounds (x=0, 0.4, 0.55, 0.8, and 2) recorded at T=295 K.

straightforward on the basis of their relative area; however, it is not easy to predict the relative values of B_{hf} at these sites. On the basis of the near neighbor environment (Z_{Fe} and Z_B) one would expect $B_{hf}(16k_1) > B_{hf}(8j_1) > B_{hf}(4e)$ but, in practice, it is found that the values of $B_{hf}(16k_1)$, $B_{hf}(8j_1)$, and $B_{hf}(4e)$ are very similar.[30–33] Moreover, their hierarchy is different depending on both the particular compound and the fitting procedure.[30–33] These small discrepancies may be due to the influence of the different Wigner-Seitz volumes (the $16k_1$ has the smallest V_{WS}), and also to the influence of the rare earth (the $8j_1$ site has four R-atom near neighbors while the $16k_1$ and the $4e$ sites have only two R near neighbors).

In the present case we have applied a similar fitting procedure to that described in Ref. 30. Each sextet is defined by its relative area, linewidth, hyperfine field, B_{hf}, isomer shift, δ, quadrupole interaction, $eQV_{zz}/2$, and the angle, θ, between the principal axis of the electric field gradient and the magnetic hyperfine field that is assumed parallel to the easy axis of magnetization. The relative area of each sextet has been kept fixed and equal to 4:4:2:2:1:1 for the $16k_1$, $16k_2$, $8j_1$, $8j_2$, $4c$, and $4e$ Fe sites, respectively. The linewidth, Γ, has been determined from the fit of the most external peak at $\sim$6 mm/s (Γ=0.27 mm/s), and it has been kept constant and identical for each sextet. The fitting process has been performed in two steps. First, we have determined the hyperfine parameters of the more intense and well defined $16k_1$, $16k_2$, and $8j_2$ sextets and, secondly, those of less well defined $8j_1$, $4c$, and $4e$ sextets. The corresponding hyperfine parameters are given in Table III. It should be noted that our fitting model only allows us to determine the value of the quadrupole shift $\epsilon=(eQV_{zz}/2)\left(\frac{3\cos^2\theta-1}{2}\right)$. According to previous works[30,32] the θ angles are 17.8, 32.9, 2.5, 11.5, 0, and 90 for the $16k_1$, $16k_2$, $8j_1$, $8j_2$, $4c$, and $4e$ Fe sites, respectively, if the hyperfine field is along the c axis. Provided that for all the studied $Nd_{2-x}Ho_xFe_{14}B$ compounds both EMD and B_{hf} lie along the [001] direction, we have used the values of θ given above to determine $eQV_{zz}/2$.

The obtained hyperfine parameters, summarized in Table III, are in agreement with those previously reported for $R_2Fe_{14}B$ compounds.[30–32] In particular, we have observed that the largest absolute values of the quadrupole interaction are found for the $8j_2$ and $4e$ sites, which is consistent with the very asymmetric electronic environment of these sites.[30] As shown in Table III all the hyperfine parameters (B_{hf}, δ, and $eQV_{zz}/2$) slightly decrease when increasing the Ho content. The total Fe average hyperfine field, $\langle B_{hf}\rangle$, of the $Nd_{2-x}Ho_xFe_{14}B$ compounds is shown in Fig. 5 as a function of the Ho concentration and compared to that of $Y_2Fe_{14}B$ obtained under the same experimental conditions. As we can see in this figure $\langle B_{hf}\rangle$ decreases linearly with x, and an anomalous reduction is observed for the x=0.55 concentration. Making a parallel to the two sublattices model for the magnetization $\langle B_{hf}\rangle$ has been calculated as a linear combination of the end-member values according to $(2-x)\times\langle B_{hf}(Nd_2Fe_{14}B)\rangle + x\langle B_{hf}(Ho_2Fe_{14}B)\rangle$ expression. The comparison of the experimental data to the calculated ones shows a good agreement with the exception of $Nd_{1.45}Ho_{0.55}Fe_{14}B$ for which $\langle B_{hf}\rangle$ suddenly departs from the linear trend. In principle, this anomalous reduction may be related with the anomalous variation of the volume. However, as shown in Fig. 5(b), there is no direct relationship between $\langle B_{hf}\rangle$ and V. Consequently, this result indicates that the anomalous variation of $\langle B_{hf}\rangle$ at x=0.55 is not of steric origin.

In all the $Nd_{2-x}Ho_xFe_{14}B$ compounds, the total Fe average hyperfine field is greater than that of $Y_2Fe_{14}B$, i.e., of the compound in which no magnetic rare earth is present. Indeed, the excess in $\langle B_{hf}\rangle$ in the former compounds is due to the rare-earth sublattice contribution to B_{hf}, the so called rare-earth transferred field, B_{tR}. Therefore, B_{hf} also probes a magnetic contribution coming from the rare-earth atoms present in the material under study. In a recent work, the variation of $\langle B_{hf}\rangle$ along the $RFe_{11.5}Ta_{0.5}$ series has been explained in terms of the rare-earth transferred field.[35] According to this model, $\langle B_{hf}\rangle$ can be written as

$$\langle B_{hf}\rangle = \langle B_{Fe}\rangle + \langle B_{tR}\rangle, \quad (1)$$

where $\langle B_{Fe}\rangle$ represents the contribution coming from the iron sublattice, and $\langle B_{tR}\rangle$ represents the contribution coming from the rare-earth sublattice. Within this model the $\langle B_{Fe}\rangle$ term is assumed to be the same for all the members of a given series

TABLE III. Room temperature hyperfine parameters of the $Nd_{2-x}Ho_xFe_{14}B$ compounds. The values of the isomer shifts are relative to α-Fe at room temperature. (In all the cases the estimated errors are at most ±0.05 T for B_{hf}, ±0.010 mm/s for δ, and ±0.020 mm/s for $eQV_{zz}/2$.)

		Site						
Hyp. Par.	x	$16k_1$	$16k_2$	$8j_1$	$8j_2$	$4c$	$4e$	Aver.
B_{hf}(T)	0	28.9	30.8	28.1	34.5	25.6	28.9	29.9
	0.2	28.9	30.7	28.0	34.5	25.6	28.9	29.8
	0.4	28.8	30.6	27.9	34.4	25.6	28.9	29.7
	0.5	28.7	30.5	27.8	34.4	25.6	28.9	29.7
	0.55	28.6	30.4	27.7	34.2	25.5	28.8	29.6
	0.6	28.7	30.5	27.8	34.4	25.6	28.9	29.7
	0.8	28.7	30.4	27.7	34.4	25.6	28.8	29.6
	1.2	28.6	30.2	27.5	34.3	25.6	28.9	29.5
	2	28.5	29.9	27.1	34.2	25.6	28.7	29.3
	$Y_2Fe_{14}B$	27.7	29.0	28.1	33.0	25.2	26.2	28.6
δ (mm/s)	0	−0.040	−0.128	−0.080	0.073	−0.109	−0.042	−0.060
	0.2	−0.048	−0.128	−0.071	0.075	−0.116	−0.044	−0.061
	0.4	−0.047	−0.126	−0.073	0.068	−0.132	−0.024	−0.061
	0.5	−0.051	−0.128	−0.078	0.068	−0.117	−0.024	−0.063
	0.55	−0.050	−0.125	−0.077	0.067	−0.121	−0.029	−0.062
	0.6	−0.050	−0.128	−0.078	0.065	−0.120	−0.033	−0.064
	0.8	−0.054	−0.131	−0.081	0.060	−0.122	−0.018	−0.066
	1.2	−0.057	−0.130	−0.079	0.059	−0.134	−0.036	−0.069
	2	−0.060	−0.129	−0.080	0.067	−0.138	−0.030	−0.068
$eQV_{zz}/2$ (mm/s)	0	0.287	0.314	0.335	0.692	−0.173	−0.747	0.253
	0.2	0.301	0.303	0.309	0.689	−0.218	−0.725	0.248
	0.4	0.286	0.297	0.321	0.691	−0.166	−0.715	0.248
	0.5	0.293	0.306	0.302	0.699	−0.159	−0.725	0.251
	0.55	0.284	0.299	0.303	0.692	−0.161	−0.704	0.247
	0.6	0.283	0.306	0.303	0.705	−0.142	−0.710	0.252
	0.8	0.285	0.298	0.299	0.688	−0.136	−0.742	0.245
	1.2	0.277	0.303	0.295	0.694	−0.161	−0.692	0.246
	2	0.270	0.320	0.289	0.673	−0.194	−0.655	0.245

and should coincide with the value of $\langle B_{hf}\rangle$ for a $R_2Fe_{14}B$ compound in which R is nonmagnetic. $\langle B_{tR}\rangle$ stems from the polarization effects due to the rare-earth magnetic moments and, consequently, it should be proportional to the R molecular field acting on the iron atoms

$$\langle B_{tR}\rangle = \zeta \gamma_R n_{R\mathrm{Fe}} \mu_R, \tag{2}$$

where ζ is a proportionality factor which depends on the number of $4s$ spins contributing to the polarization, $\gamma_R = 2(g_J - 1)/g_J$, $n_{R\mathrm{Fe}}$ is the R-Fe exchange coefficient, and μ_R is the rare-earth magnetic moment. In the case of the $Nd_{2-x}Ho_xFe_{14}B$ compounds, we have taken

$$\langle B_{tR}\rangle = \langle B_{t\mathrm{Nd}}\rangle + \langle B_{t\mathrm{Ho}}\rangle = (2-x)\zeta \gamma_{\mathrm{Nd}} n_{\mathrm{NdFe}} \mu_{\mathrm{Nd}} + x\zeta \gamma_{\mathrm{Ho}} n_{\mathrm{HoFe}} \mu_{\mathrm{Ho}}. \tag{3}$$

We have plotted in Fig. 5(c) $\langle B_{hf}\rangle$ as a function of $(2-x)\gamma_{\mathrm{Nd}} n_{\mathrm{NdFe}} \mu_{\mathrm{Nd}} + x\gamma_{\mathrm{Ho}} n_{\mathrm{HoFe}} \mu_{\mathrm{Ho}}$. The values of the exchange parameters, n_{NdFe} and n_{HoFe}, have been calculated according to Ref. 36 and both μ_{Nd} and μ_{Ho} have been derived from the magnetization data. This analysis perfectly reproduces the observed decrease of $\langle B_{hf}\rangle$ from $Nd_2Fe_{14}B$ to $Ho_2Fe_{14}B$, with the only exception of the $x=0.55$ compound.

The inspection of Fig. 5 shows two main results: (i) the rare-earth transferred field is higher for $Nd_2Fe_{14}B$ than for $Ho_2Fe_{14}B$, in agreement with the enhanced R-Fe exchange for light-R compounds over the heavy-R ones,[12,35] and (ii) as Nd is replaced by Ho, $\langle B_{tR}\rangle$ decreases linearly with the only exception of the $x=0.55$ compound. The latter result supports that the magnetization of the Fe sublattice remains constant through the $Nd_{2-x}Ho_xFe_{14}B$ series.

The observed reduction of $\langle B_{hf}\rangle$ at $x=0.55$ can be due to the decrease of μ_{Fe}, μ_{Nd}, or μ_{Ho}. Unfortunately, it is not

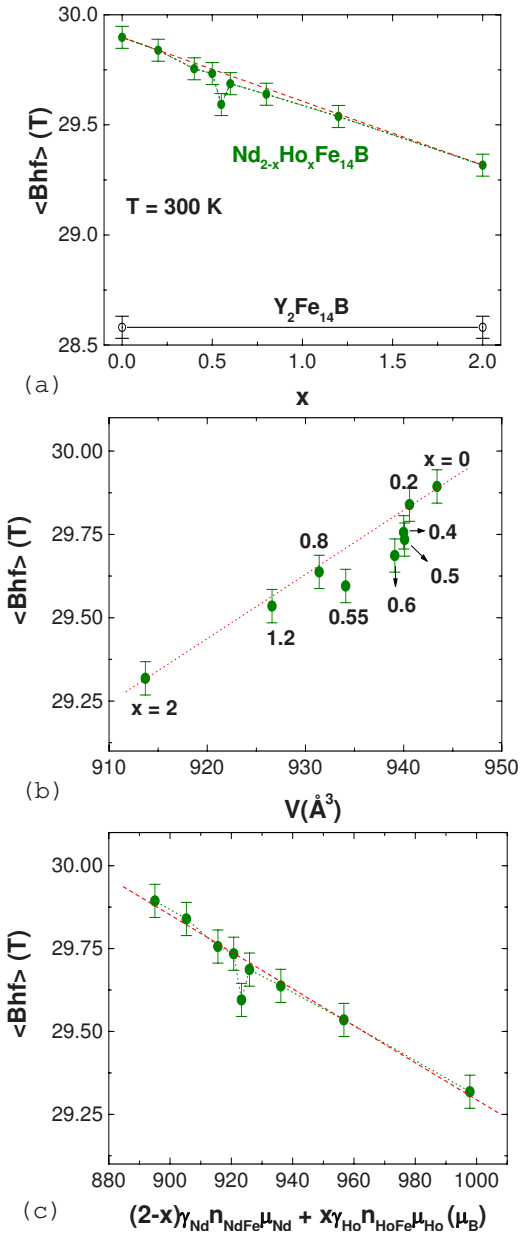

FIG. 5. (Color online) (a) Concentration dependence of the room temperature Fe average hyperfine field through the $Nd_{2-x}Ho_xFe_{14}B$ series (green, ●). For the sake of completeness $\langle B_{hf}\rangle$ of $Y_2Fe_{14}B$ is also shown (black, ○). The dashed line corresponds to the $\langle B_{hf}\rangle$ calculated as a linear combination of the end-member values. (b) Cell-volume dependence of $\langle B_{hf}\rangle$ (the dotted line is a guide to the eye). (c) $\langle B_{hf}\rangle$ vs $(2-x)\gamma_{Nd}n_{NdFe}\mu_{Nd}+x\gamma_{Ho}n_{HoFe}\mu_{Ho}$: experimental (green, ●) and theoretically calculated (red, dashed line) (see text for details).

possible to learn further on the origin of the peculiar behavior at this concentration from the analysis of the $\langle B_{hf}\rangle$ data only. The rare-earth contribution to $\langle B_{hf}\rangle$ does not reflect the different magnetic coupling among the Nd (ferro-) and Ho (ferri-) magnetic moments with the Fe moment. However, the combined analysis of both $\langle B_{hf}\rangle$ and magnetization data suggests that this behavior may be mainly addressed to the Ho sublattice. Indeed, the magnetization of $Nd_{1.45}Ho_{0.55}Fe_{14}B$ increases while it should decrease if either μ_{Fe} or μ_{Nd} decreases. This result points out that it is the contribution of the Ho sublattice to the total magnetization of the system which anomalously decreases for the $x=0.55$ concentration. This proposition is compatible with both the observed decrease of $\langle B_{hf}\rangle$ and the increase of M_R occurring for this concentration.

C. Fe *K*-edge x-ray magnetic circular dichroism

The qualitative analysis above suggests a different behavior of the Ho sublattice with respect to the Nd and Fe ones near the critical concentration for the compensation of the macroscopic rare-earth magnetization through the $Nd_{2-x}Ho_xFe_{14}B$ series. Aimed to verify this finding we have performed an XMCD study of the Fe *K*-edge signal in these compounds. The main advantage of using XMCD lies in its atomic selectivity. Moreover, it has been proposed that even if there is a contribution coming from the rare-earth atoms, this contribution reflects also, contrary to B_{tR}, the coupling of the magnetic moments. Therefore, the study of the XMCD may lead to a deeper insight of the different magnetic behavior of the three sublattices close to the critical $x=0.55$ concentration.

The comparison of the Fe *K*-edge XMCD spectra of $Y_2Fe_{14}B$, $Nd_2Fe_{14}B$, and $Ho_2Fe_{14}B$ is reported in Fig. 6. The Fe *K*-edge spectrum of $Y_2Fe_{14}B$ is characterized by a narrow positive peak (*A*) at the absorption edge ($E-E_0=1$ eV) followed by a broad negative dip (~12 eV wide). This shape is similar to that of Fe metal.[1] By contrast, the spectral profile of the Fe *K*-edge XMCD of both $Nd_2Fe_{14}B$ and $Ho_2Fe_{14}B$ compounds is quite different with respect to that of $Y_2Fe_{14}B$. In principle, one expects a close similarity of their XMCD signals because (i) the three compounds exhibit the same crystal structure (and thus similar local Fe environment), (ii) it is usually accepted that Fe *K*-edge XMCD probes only the Fe atoms in these materials, and (iii) the magnetic properties of the Fe sublattice in these compounds are thought to be nearly identical.[12] However, this is not the case. While both $Nd_2Fe_{14}B$ and $Ho_2Fe_{14}B$ show the narrow peak at the edge (*A*), the higher energy region is significantly modified, both in sign and amplitude, with respect to $Y_2Fe_{14}B$. In the case of $Nd_2Fe_{14}B$ the former negative dip in $Y_2Fe_{14}B$ splits into two intense peaks of negative (*B*) and positive (*B'*) sign located at energies 5 and 14 eV above the edge, respectively. The $Ho_2Fe_{14}B$ XMCD spectrum shows a negative intense peak at 3 eV (*C*), a broad positive one at 7 eV (*C'*), and a second negative peak (*C''*) centered at ~12 eV above the edge.

The strong dependence of the Fe *K*-edge XMCD spectra in *R*-Fe compounds on the specific nature of the rare earth has been previously assigned to the magnetic contribution of the rare earth even if Fe atoms are being probed.[7–11] As discussed previously in detail (see, for example, Ref. 7) the Fe *K*-edge absorption in *R*-Fe intermetallic materials can be sensitive also to the lanthanide 5*d* states through the hybridization of the outermost states of the absorbing Fe with the 5*d* states of the rare-earth neighbors. Accordingly, the total XMCD signal can be expressed as the addition of two components: $XMCD_{tot}=XMCD_{Fe}+XMCD_R$, being $XMCD_R$ and

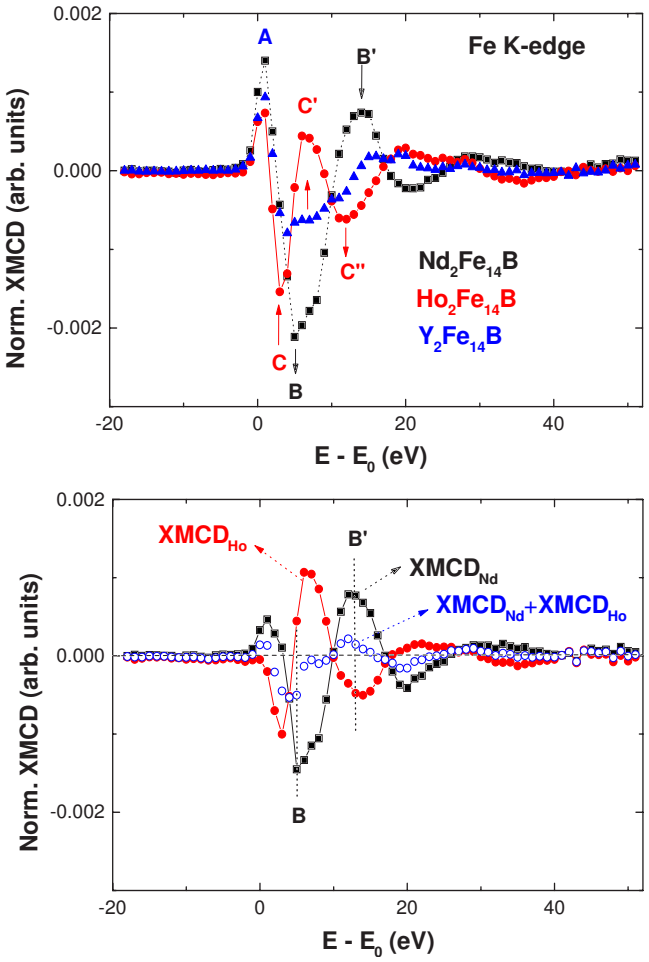

FIG. 6. (Color online) Top panel: room temperature Fe *K*-edge XMCD spectra of $Nd_2Fe_{14}B$ (black, ■), $Ho_2Fe_{14}B$ (red, ●), and $Y_2Fe_{14}B$ (blue, ▲). Bottom panel: comparison of the XMCD signals obtained after subtracting the Fe *K*-edge XMCD spectrum of $Y_2Fe_{14}B$ to that of $Nd_2Fe_{14}B$, $XMCD_{Nd}$ (black, ■), $Ho_2Fe_{14}B$, $XMCD_{Ho}$ (red, ●), and their addition $XMCD_{Nd}+XMCD_{Ho}$ (blue, ○).

$XMCD_{Fe}$ the magnetic contributions of the rare earth and Fe magnetic sublattices, respectively. Making a parallel to the two-sublattice analysis of the magnetization data, the difference signal defined as $XMCD_{diff}=XMCD\ (Nd_{2-x}Ho_xFe_{14}B) - XMCD\ (Y_2Fe_{14}B)$ would correspond to the rare-earth contribution to the Fe *K*-edge XMCD spectra through the $Nd_{2-x}Ho_xFe_{14}B$ series. This procedure is illustrated in Fig. 6 for both $Nd_2Fe_{14}B$ and $Ho_2Fe_{14}B$ compounds. As shown in the figure (top panel), the amplitude of the signals associated with both Nd and Ho are of the same order of magnitude as for $Y_2Fe_{14}B$. This result indicates that the contribution of the rare earth to the Fe *K* edge is not a simple correction to the Fe one but it determines the shape of the signal. Moreover, the sign of this rare-earth contribution depends on the coupling between the rare-earth magnetic moment and the Fe one. This is illustrated in Fig. 6 (bottom panel) where it is shown that the contribution of Nd and Ho ($XMCD_{diff}$) are of similar amplitude but of opposite sign, as corresponding to the different magnetic coupling between μ_{Nd} (ferro-) and μ_{Ho} (ferri-) with μ_{Fe} in $Nd_2Fe_{14}B$ and $Ho_2Fe_{14}B$, respectively.

The importance of this result lies into the possibility of using the Fe *K*-edge XMCD in *R*-Fe intermetallics as a selective magnetometry probe of the rare-earth magnetism. In principle, one can conclude that since the overall XMCD signal corresponds to the combination of the Fe and *R* moments, the XMCD resembles the macroscopic (bulk) measurements. In other words, that the existence of Fe-*R* hybridization makes Fe *K*-edge XMCD equivalent to various bulk probes. However, the detailed study of the XMCD signals shows that the effect of the rare earth is not equivalent to that of an effective rare-earth magnetization but it conserves the atomic nature and the characteristic magnetic coupling of each rare-earth species. In other words, both Nd and Ho contribute according to their magnetic moment value and coupling, independently of the averaged M_R.

To verify this possibility we have proceeded in the following way: (i) as discussed above, we have extracted the contribution of the Nd atoms to the Fe *K*-edge XMCD of $Nd_2Fe_{14}B$ by subtracting to its XMCD spectrum that of $Y_2Fe_{14}B$, $XMCD_{diff}(Nd)=XMCD(Nd_2Fe_{14}B) - XMCD(Y_2Fe_{14}B)$; (ii) a similar procedure is made on $Ho_2Fe_{14}B$, $XMCD_{diff}(Ho)=XMCD(Ho_2Fe_{14}B) - XMCD(Y_2Fe_{14}B)$; (iii) in doing this we are assuming that the Fe magnetization does not significantly vary in both compounds; and (iv) then, the Fe *K*-edge XMCD of the different $Nd_{2-x}Ho_xFe_{14}B$ compounds, $XMCD_{tot}$, is reconstructed as

$$XMCD_{tot} = XMCD(Y_2Fe_{14}B) + (2-x)\ XMCD_{diff}(Nd) + x\ XMCD_{diff}(Ho).$$

This simple addition incorporates the ferro-(ferri-) magnetic coupling of the Nd(Ho) magnetic moments to that of Fe. The result of such a procedure is shown in Fig. 7. The agreement between the experimental spectra and those built up from the individual (Fe, Nd, and Ho) signals is remarkable. In addition, the fact that all the spectra, both experimental and theoretically reconstructed, cross at the same energy points (P1, P2, and P3, see Fig. 7) supports the validity of our hypothesis. Moreover, it should be noted that the rare-earth XMCD contribution does not become zero as the averaged M_R does in the neighboring of the compensation of the rare-earth sublattice magnetization, M_R. However, the agreement worsens in the case of the $Nd_{1.45}Ho_{0.55}Fe_{14}B$ compound. This result indicates that our approach breaks down for this particular concentration. Then, either the Nd or the Ho contribution to the Fe *K*-edge XMCD departs from the expected value.

The integrated Fe *K*-edge XMCD has been compared to the rare-earth magnetization in Fig. 8. This comparison shows that, as expected, the overall XMCD signal corresponds to the combination of the Fe and rare-earth moments resembling the macroscopic magnetization. Indeed, the sudden increase of M_R at $x=0.55$ is reproduced by the integrated XMCD signals. However, it is possible to take advantage of the different energy dependence of the individual Nd and Ho contributions extracted from the XMCD signals to disentangle its modification through the $Nd_{2-x}Ho_xFe_{14}B$ series. As

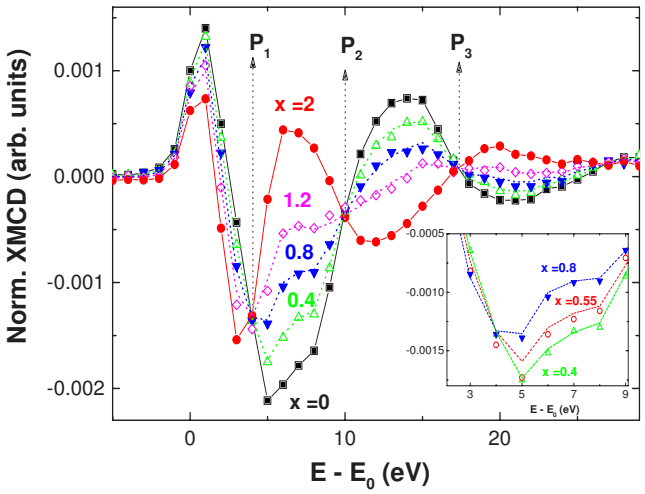

FIG. 7. (Color online) Fe *K*-edge XMCD spectra of the $Nd_{2-x}Ho_xFe_{14}B$ compounds as a function of the Ho concentration: $x=0$ (black, ■), $x=0.4$ (green, △), $x=0.8$ (blue, ▼), $x=1.2$ (magenta, ◇), and $x=2$ (red, ●). The dotted lines correspond to the XMCD spectra obtained as the weighted sum of the XMCD signals of both $Nd_2Fe_{14}B$ and $Ho_2Fe_{14}B$ (see text for details). In the inset, a magnified view of the same comparison in the case of $x=0.4$ (green, △), $x=0.8$ (blue, ▼), and $x=0.55$ (red, ○) is shown.

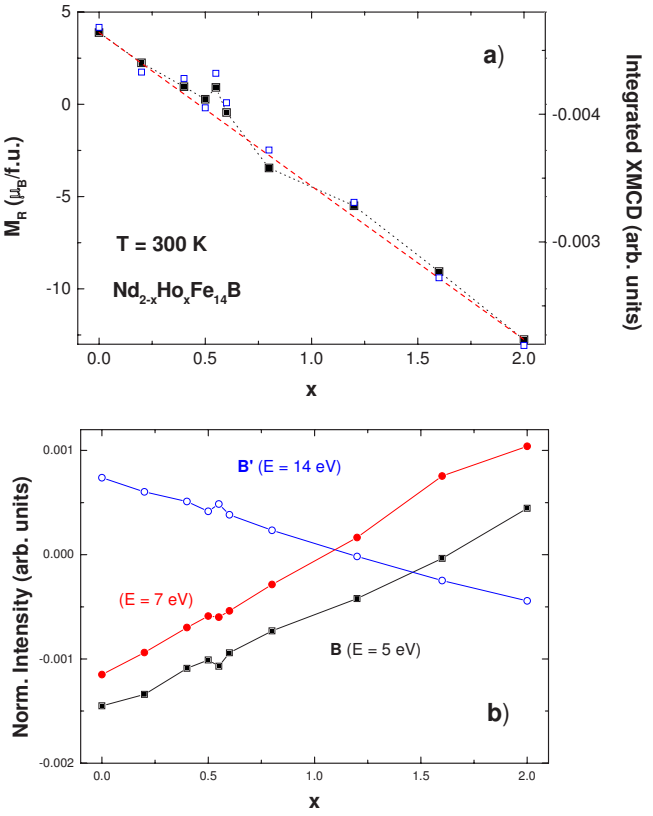

FIG. 8. (Color online) Top panel: comparison between the rare-earth sublattice magnetization of the $Nd_{2-x}Ho_xFe_{14}B$ compounds derived from $M(H)$ curves (black, ■) and the integrated Fe *K*-edge XMCD signals (blue, □). Bottom panel: comparison of the intensity of the main absorption peaks of the XMCD signals obtained after subtracting the $Y_2Fe_{14}B$ XMCD spectrum to that of the $Nd_{2-x}Ho_xFe_{14}B$ compounds (see text for details): *B* (5 eV) (black, ■), (7 eV) (red, ●), and *B'* (14 eV) (blue, ○).

shown in Fig. 6, the main peaks of the Nd contribution lie at 5 eV (peak *B*) and 14 eV (*B'*) being negative and positive, respectively. At these energies, the sign of the Nd contribution dominates over the Ho one. Therefore, we have plotted the variation of the XMCD intensity at these energies as a function of the Ho concentration. The result, reported in Fig. 8, shows that for $x=0.55$ the intensity of peak *B* becomes more negative and the contrary occurs at *B'*. A similar result is obtained when examining the intensity of the XMCD spectra at an energy in which the contribution of both Nd and Ho cancels. At $E=7$ eV the positive contribution of Ho cancels the negative one of Nd to the total XMCD. As the Ho concentration increases one expects that the XMCD intensity increases but the contrary is experimentally observed. These results indicate that either the Nd contribution increases or the Ho contribution decreases. However, the observed reduction of the rare-earth sublattice contribution to B_{hf}, to which both Nd and Ho contributes positively, is only compatible with the reduction of the Ho contribution to the total magnetization, B_{hf}, and XMCD.

These results address that the anomalous behavior of $Nd_{1.45}Ho_{0.55}Fe_{14}B$ within the $Nd_{2-x}Ho_xFe_{14}B$ series lies in the anomalous magnetic behavior of the Ho sublattice. According to steric considerations Ho preferentially substitutes Nd at the 4*f* sites and, in addition, the *R*-Fe exchange fields significantly differ for the inequivalent 4*f* and 4*g* sites.[37] Moreover, it has been recently demonstrated that the 4*g* sites are predominately responsible for the intrinsic magnetic coercivity of $Nd_2Fe_{14}B$ (Ref. 20) as the *R*-Fe exchange coupling is not strong enough to ensure a rigid rotation of Nd and Fe magnetizations.[18–20] Consequently, the peculiar behavior of the Ho sublattice may be due to a canting of the Ho magnetic moments resulting from the interplay of both the competing interactions at the 4*f* and 4*g* sites associated with the preferential occupancy and to the occurrence of a compensation of the rare-earth sublattice magnetization.

IV. SUMMARY AND CONCLUSIONS

We have reported here the systematic study of the $Nd_{2-x}Ho_xFe_{14}B$ series performed by means of XRD, macroscopic magnetization, ^{57}Fe Mössbauer spectroscopy, and Fe *K*-edge XMCD.

The macroscopic properties of the $Nd_{2-x}Ho_xFe_{14}B$ compounds evolve continuously from those of $Nd_2Fe_{14}B$ to those of $Ho_2Fe_{14}B$ as the Ho concentration increases. However, for a critical concentration $x_c=0.55$ the system presents an anomalous behavior that is reflected in both macroscopic (XRD and magnetization) and microscopic (^{57}Fe Mössbauer and XMCD) probes. For this concentration the system is close to the magnetic compensation of the rare-earth sublattice due to the competition between the ferrimagnetically coupled Nd and Ho magnetic moments. The combined analysis of both magnetization and Mössbauer measurements suggests a different behavior of the Ho sublattice with respect to the Nd and Fe ones near the critical concentration.

The analysis of the Fe *K*-edge XMCD data confirms previous findings regarding the existence of a contribution com-

ing from the rare-earth atoms even if Fe atoms are being probed. The comparison of the integrated XMCD spectra and the magnetization shows that the overall XMCD signal corresponds to the combination of the Fe and rare-earth moments so as to resemble the macroscopic magnetization. Contrary to the case of ^{57}Fe Mössbauer spectroscopy, the rare-earth contribution to the Fe *K*-edge XMCD reflects the coupling of the rare-earth magnetic moments.

The detailed study of the XMCD signals shows that the rare-earth contribution is not equivalent to that of an effective rare-earth magnetization but it conserves the atomic nature and the characteristic magnetic coupling of each rare-earth species. Both Nd and Ho contribute according to their magnetic moment value, the sign of its coupling with the Fe magnetic moment, and the averaged number of Nd(Ho) neighbors to Fe at a given concentration (x), independently of the averaged rare-earth sublattice magnetization. The amplitude of the Nd and Ho contribution to the XMCD spectrum is maximized at different energies and, by monitoring the XMCD intensity at these positions, it is possible to disentangle the magnetization of both rare-earth sublattices. These results point out that the origin of the anomalous magnetic behavior of the $Nd_{2-x}Ho_xFe_{14}B$ compounds at a critical concentration $x_c=0.55$ is mainly due to the Ho sublattice.

These results open the possibility of using the Fe *K*-edge XMCD in *R*-Fe intermetallics as a selective magnetometry probe of both Fe and rare-earth magnetism. By fixing the energy at the adequate positions of a single XMCD spectrum it would be possible to record hysteresis cycles corresponding to the transition metal and to the rare-earth separately. We think that these results can stimulate further research to demonstrate the capability of XMCD of providing selective magnetometry of different atomic species at a single absorption edge.

ACKNOWLEDGMENTS

This work was partially supported by Spanish CICYT-MAT2005-06806-C04-04 grant. M. A. L.-M. acknowledges a FPI grant from spanish MEC. The synchrotron radiation experiments were performed at SPring-8 (Proposal No. 2002A0153-NS2-np). We are indebted to N. Kawamura and H. Maruyama for their help during the experimental work at SPring8.

*Also at: National Institute of Materials Physics, P.O. Box MG-07, Bucharest-Magurele 77125, Romania

[1] G. Schütz, W. Wagner, W. Wilhelm, P. Kienle, R. Zeller, R. Frahm, and G. Materlik, Phys. Rev. Lett. **58**, 737 (1987).
[2] B. T. Thole, P. Carra, F. Sette, and G. van der Laan, Phys. Rev. Lett. **68**, 1943 (1992).
[3] P. Carra, B. T. Thole, M. Altarelli, and X. Wang, Phys. Rev. Lett. **70**, 694 (1993).
[4] X. Wang, T. C. Leung, B. N. Harmon, and P. Carra, Phys. Rev. B **47**, 9087 (1993).
[5] J. C. Lang, S. W. Kycia, X. D. Wang, B. N. Harmon, A. I. Goldman, D. J. Branagan, R. W. McCallum, and K. D. Finkelstein, Phys. Rev. B **46**, 5298 (1992).
[6] J. Chaboy, F. Bartolomé, L. M. García, and G. Cibin, Phys. Rev. B **57**, R5598 (1998).
[7] M. A. Laguna-Marco, J. Chaboy, and H. Maruyama, Phys. Rev. B **72**, 094408 (2005).
[8] J. Chaboy, H. Maruyama, L. M. García, J. Bartolomé, K. Kobayashi, N. Kawamura, A. Marcelli, and L. Bozukov, Phys. Rev. B **54**, R15637 (1996).
[9] J. Chaboy, L. M. García, F. Bartolomé, H. Maruyama, A. Marcelli, and L. Bozukov, Phys. Rev. B **57**, 13386 (1998).
[10] J. Chaboy, C. Piquer, N. Plugaru, M. Artigas, H. Maruyama, N. Kawamura, and M. Suzuki, J. Appl. Phys. **93**, 475 (2003).
[11] J. Chaboy, M. A. Laguna-Marco, M. C. Sánchez, H. Maruyama, N. Kawamura, and M. Suzuki, Phys. Rev. B **69**, 134421 (2004).
[12] J. F. Herbst and J. J. Croat, Rev. Mod. Phys. **63**, 819 (1991).
[13] E. Burzo, Rep. Prog. Phys. **61**, 1099 (1998).
[14] K. Kobayashi and S. Hirosawa, in *Handbook on the Physics and Chemistry of Rare Earths*, edited by K. A. Gschneider, Jr., L. Eyring, and G. H. Lander (Elsevier, Amsterdam, 2002), Vol. 32, Chap. 208.
[15] *Handbook of Advanced Magnetic Materials*, edited by Y. Liu, D. J. Sellmyer, and D. Shindo (Springer, New York, 2006).
[16] M. Sagawa, S. Fujimura, H. Yamamoto, Y. Matsuura, and S. Hirosawa, J. Appl. Phys. **57**, 4094 (1985).
[17] S. Hirosawa, Y. Matsuura, H. Yamamoto, S. Fujimura, M. Sagawa, and H. Yamauchi, J. Appl. Phys. **59**, 873 (1986).
[18] J. Chaboy *et al.*, Phys. Rev. B **57**, 8424 (1998).
[19] F. Bartolomé, J. M. Tonnerre, N. Jaouen, D. Raoux, J. Chaboy, L. M. García, H. Maruyama, and R. Steinmann, J. Appl. Phys. **87**, 4762 (2000).
[20] D. Haskel, J. C. Lang, Z. Islam, A. Cady, G. Srajer, M. van Veenendaal, and P. C. Canfield, Phys. Rev. Lett. **95**, 217207 (2005).
[21] J. Rodriguez-Carvajal, Physica B **192**, 55 (1993).
[22] H. Maruyama, J. Synchrotron Radiat. **8**, 125 (2001).
[23] K. Hirano, K. Izumi, T. Ishikawa, S. Annaka, and S. Kikuta, Jpn. J. Appl. Phys., Part 2 **30**, L407 (1991).
[24] M. Suzuki, N. Kawamura, M. Mizumaki, A. Urata, H. Maruyama, S. Goto, and T. Ishikawa, Jpn. J. Appl. Phys., Part 2 **37**, L1488 (1998).
[25] D. E. Sayers and B. A. Bunker, in *X-Ray Absorption: Principles, Applications, Techniques of EXAFS, SEXAFS, and XANES*, edited by D. C. Koningsberger and R. Prins (Wiley, New York, 1988), Chap 6, and references therein.
[26] H. Yamauchi, H. Hiroyoshi, Y. Yamaguchi, H. Yamamoto, M. Sagawa, Y. Matsuura, and H. Yamamoto, J. Magn. Magn. Mater. **49**, 210 (1985).
[27] A. T. Pedziwiatr, W. E. Wallace, and E. Burzo, J. Magn. Magn. Mater. **61**, 173 (1986).
[28] J. F. Herbst and J. J. Croat, J. Appl. Phys. **55**, 3023 (1984).
[29] It should be noted that we use M_{tot} (5 T) values instead of saturation magnetization estimates to allow a direct comparison with the XMCD data recorded at the same applied field.
[30] F. Grandjean, G. J. Long, O. A. Pringle, and J. Fu, Hyperfine

Interact. **62**, 131 (1990).
[31] H. Onodera, A. Fujita, H. Yamamoto, M. Sagawa, and S. Hirosawa, J. Magn. Magn. Mater. **68**, 6 (1987).
[32] G. J. Long, R. Kulasekere, O. A. Pringle, F. Grandjean, and K. H. J. Buschow, J. Magn. Magn. Mater. **117**, 239 (1992).
[33] D. E. Tharp, G. J. Long, O. A. Pringle, G. K. Marasinghe, W. J. James, and F. Grandjean, J. Appl. Phys. **64**, 5583 (1988).
[34] M. Shiga, in *Magnetic Properties of Metals*, Landolt-Börnstein, New Series Group III, edited by H. P. J. Wijn (Springer-Verlag, Berlin, 1986), Chap. 1.
[35] C. Piquer, J. Rubín, J. Bartolomé, V. Kuncser, and G. Filoti, Phys. Rev. B **73**, 174433 (2006).
[36] N. Plugaru, J. Rubín, J. Bartolomé, C. Piquer, and M. Artigas, Phys. Rev. B **65**, 134419 (2002).
[37] M. Loewenhaupt, I. Sosnowska, A. Taylor, and R. Osborn, J. Appl. Phys. **69**, 5593 (1991).